Crystal Structure of the Potent Natural Product Inhibitor Balanol in Complex with the Catalytic Subunit of cAMP-Dependent Protein Kinase†

Narendra Narayana,[‡,§] Thomas C. Diller,[‡,||] Kazunori Koide,[‡,§] Mark E. Bunnage,[‡,§] K. C. Nicolaou,[‡,⊥] Laurence L. Brunton,[#] Nguyen-Huu Xuong,[‡,▽] Lynn F. Ten Eyck,[○] and Susan S. Taylor*[,‡,||]

The Howard Hughes Medical Institute and Departments of Biology, Chemistry and Biochemistry, Pharmacology, and Physics, University of California, San Diego, 9500 Gilman Drive, La Jolla, California, Department of Chemistry, The Scripps Research Institute, 10666 North Torrey Pines Road, La Jolla, California, and the Science Department, San Diego Supercomputer Center, La Jolla, California

Received August 25, 1998; Revised Manuscript Received October 22, 1998

ABSTRACT: Endogenous protein kinase inhibitors are essential for a wide range of physiological functions. These endogenous inhibitors may mimic peptide substrates as in the case of the heat-stable protein kinase inhibitor (PKI), or they may mimic nucleotide triphosphates. Natural product inhibitors, endogenous to the unique organisms producing them, can be potent exogenous inhibitors against foreign protein kinases. Balanol is a natural product inhibitor exhibiting low nanomolar K_i values against serine and threonine specific kinases, while being ineffective against protein tyrosine kinases. To elucidate balanol's specific inhibitory effects and provide a basis for understanding inhibition-regulated biological processes, a 2.1 Å resolution crystal structure of balanol in complex with cAMP-dependent protein kinase (cAPK) was determined. The structure reveals conserved binding regions and displays extensive complementary interactions between balanol and conserved cAPK residues. This report describes the structure of a protein kinase crystallized with a natural ATP mimetic in the absence of metal ions and peptide inhibitor.

Protein kinases, of which the human genome is predicted to encode several thousand, reversibly phosphorylate diverse molecular targets and are critical enzymes in the initiation, regulation, and abrogation of both normal and abnormal cellular functions (reviewed in refs *1*−*6*). These often exquisitely specific kinases play essential roles in apoptosis, cell proliferation, gene expression, glycogen metabolism, immune response, neurotransmission, oncogenesis, and secondary messenger signal transduction (*7*−*18*). This biological pervasiveness underscores the importance of more explicitly characterizing kinase activation and inhibition. Additionally, there is significant therapeutic value in achieving selective pharmacological control of members of this important class of enzymes, since unregulated or otherwise defective protein kinase activities to date have been implicated in asthma, cancer, cardiovascular disorders, central nervous system (CNS)[1] diseases, diabetes, human immunodeficiency virus (HIV) infections, inflammation, psoriasis, and rheumatoid arthritis (*19*−*24*).

To more explicitly characterize protein kinase activation and inhibition, cAMP-dependent protein kinase, the most completely characterized and mechanistically simplest protein kinase (*25*, reviewed in refs *26*−*31*), is a logical singular choice for biochemical and structural research focusing on cellular phosphorylation events at the molecular level. The inactive cAPK holoenzyme consists of two regulatory (R) and two catalytic (C) subunits that dissociate in response to elevated levels of intracellular cAMP. The triply phosphorylated, active C subunit then phosphorylates serine or threonine residues of peptide substrates containing the consensus sequence Arg-Arg-X-Ser[Thr]-Hyd, where X is variable and Hyd is any hydrophobic residue (*3*, *14*, *32*, *33*). The C subunit of cAPK shares with other kinase family members a conserved catalytic core of approximately 260 amino acids and 11 invariant residues (*1*). A three-dimensional description of this catalytic core became available when the first crystal structure of a protein kinase, the

△ Atomic coordinates have been deposited with the Brookhaven PDB (accession number 1bx6).

* Corresponding author.

† Work supported by National Institutes for Health Grants (GM19301 to S.S.T.; RR01664 and RR10748 to N.-H.X.) and the Howard Hughes Medical Institute. T.C.D. was supported by predoctoral fellowships from the Lucille P. Markey Charitable Trust and the National Science Foundation.

‡ Department of Chemistry and Biochemistry, University of California, San Diego.

§ Present addresses: N.N., Department of Biochemistry and Molecular Biology, University of Chicago, 924 East 57th Street, R312, Chicago, IL 60637; K.K., Department of Chemistry and Chemical Biology, Harvard University, 12 Oxford Street, Cambridge, MA 02138; M.E.B., Pfizer Central Research, Sandwich, CT13 9NJ, U.K.

|| Howard Hughes Medical Institute, School of Medicine, University of California, San Diego.

⊥ Department of Chemistry, The Scripps Research Institute.

Department of Pharmacology, School of Medicine, University of California, San Diego.

▽ Departments of Biology and Physics, University of California, San Diego.

○ Science Department, San Diego Supercomputer Center.

[1] Ade, adenosine; C, catalytic; cAPK, cAMP-dependent protein kinase; cdk, cyclin-dependent kinase; CNS, central nervous system; FGF, fibroblast growth factor; H, hydrogen; HIV, human immunodeficiency virus; HOH, water; Hyd, hydrophobic; mC, mammalian catalytic; MPD, 2-methyl-2,4-pentanediol; PDB, protein data bank; PEG, poly(ethylene glycol); PKC, phospholipid-dependent protein kinase; PKG, cGMP-dependent protein kinase; PKI, protein kinase inhibitor; R, regulatory; rC, recombinant mouse catalytic; Tris-HCl, tris(hydroxymethyl)aminomethane hydrochloride; VDW, van der Waals.

10.1021/bi9820659 CCC: $18.00
Published on Web 02/03/1999

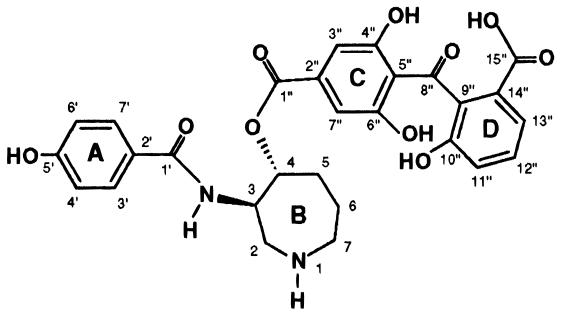

FIGURE 1: The chemical structure of balanol. The ring structures are denoted as follows: **A** = 4-hydroxybenzamide, **B** = azepane (hexahydroazepine), **C** = 3,5-dihydroxy-4-keto-benzoic acid, and **D** = 3-hydroxy-2-keto-benzoic acid. Rings C and D constitute a substituted and esterified benzophenonedioic acid. This figure was generated with ChemDraw Plus (*80*). Atom numbering is consistent with that reported previously (*81*).

recombinant mouse catalytic subunit (rC) of cAPK, was solved as a complex with PKI (residues 5−24) (*34*, *35*) and Mg_2ATP (*36*, *37*).

To further understand the detailed structural rearrangements accompanying kinase catalytic events, crystal structures of complexes involving the C subunit of cAPK subsequently were solved (*38*−*50*), as were numerous crystal structures of diverse kinases (*51*−*65*) and inhibitor−kinase complexes (*66*−*75*). Not only do these structures show how kinase core catalytic activity is affected either by endogenous inhibitors (e.g., R subunits, PKI and self-associating protein segments) or by exogenous ones (e.g., divalent metal ions, the natural product balanol and a host of synthetic analogues), they also provide greater insight into the specific interactions underlying inhibition. Detailed knowledge of the interactions between kinases and their inhibitors forms the basis of structure-based drug designs (*50*, *76*−*79*), and extensive searches for and characterizations of exogenous inhibitors continue.

Natural products increasingly are being sought and tested as templates for synthetically prepared exogenous inhibitors of protein kinases. Balanol, an ATP mimetic and one of the most potent natural product protein kinase inhibitors discovered to date, is one such template particularly amenable to analogue design. The isolation of balanol (Figure 1) may have been reported initially with the name of ophiocordin, an antifungal metabolite produced by *Cordyceps ophioglossoides* (*82*−*84*). Sixteen years after the initial characterization of ophiocordin, the absolute stereochemical structure of balanol, its isolation from *Verticillium balanoides* and its low nanomolar inhibitory effects against nearly all protein kinase C (PKC) isoforms were reported (*81*). Subsequently, azepinostatin, a *Fusarium merismoides* metabolite structurally identical to balanol, was isolated and reported to have a K_i value of 0.5 nM against rat brain PKC (*85*).

The total synthesis of balanol (*86*−*90*) and preparation of balanol derivatives now enable dissection of features underlying balanol's high affinity and selectivity for serine and threonine specific protein kinases. Recent studies indicate that balanol potently inhibits cAPK, most PKC isoforms, PKG, and Ca^{2+}-calmodulin-dependent protein kinase (*91*−*95*). Balanol, however, does not effectively inhibit other serine and threonine specific protein kinases such as casein kinase II and phosphorylase kinase or tyrosine kinases. Furthermore, large changes in isoform specificity are observed within the cAPK, PKG, and PKC families with balanol derivatives (*91*−*94*). Protein kinase specificity and the energetic determinants of inhibition by balanol and balanol derivatives are treated fully in two accompanying reports (*95*, *96*). The structure of balanol bound to the catalytic subunit of cAPK provides not only a foundation for understanding the molecular basis for balanol's high affinity but also serves as the template for further probing the specificity differences observed with balanol analogues when tested within the cAPK, PKC, and PKG family of serine and threonine specific protein kinases.

MATERIALS AND METHODS

Crystals. Crystals of balanol in complex with the active recombinant mouse C subunit−autophoshphorylated at Ser10, Thr197, and Ser338 (*33*)−were grown by hanging-drop vapor diffusion at 4 °C. The 20 μL drops consisted of 7 mg/mL protein, 0.5 mM balanol, 3% 2-methyl-2,4-pentanediol (MPD), 3% poly(ethylene glycol) (PEG) 200, and 100 mM bicine at pH 8.0. The 1 mL reservoirs consisted of 15% MPD, 10% PEG 200, and 100 mM tris(hydroxymethyl)-aminomethane hydrochloride (Tris-HCl) at pH 7.5. X-ray diffraction quality crystals measuring 0.15 × 0.20 × 0.30 mm^3 grew in 4−6 weeks. Crystals of the rC−balanol complex belong to the $P2_12_12_1$ orthorhombic space group with unit cell dimensions a = 57.19 Å, b = 73.18 Å, and c = 99.77 Å; these dimensions are isomorphous with those of the rC−adenosine (rC−Ade) complex crystals (*48*). There is one binary complex per asymmetric unit (V_m = 2.5 $Å^3$/Da, 51% solvent content).

X-ray Data Acquisition. Diffraction data were collected to 2.1 Å on two crystals at 4 °C using Xuong-Hamlin multiwire area detectors (*97*) and Cu Kα radiation (λ = 1.54 Å) from a Rigaku RU-200 rotating anode X-ray generator equipped with a graphite monochromator and operating at 5 kW power. The data were reduced with area detector data processing programs (*98*) and were 84% complete with an R_{sym} ($\Sigma|I_{obs} - I_{avg}|/\Sigma I_{avg}$) of 0.095 and a redundancy of 3.5. The Wilson B is 24 $Å^2$ for 20−2.1 Å data.

Structure Solution and Crystallographic Refinement. The atomic coordinates of the rC−Ade binary complex, Brookhaven Protein Data Bank (PDB) entry 1bkx, were used as the starting model. The isotropic thermal factors were set uniformly to 25 Å for all protein atoms. The model was initially subjected to rigid body refinement followed by several cycles of conjugate-gradient positional, overall isotropic, and individual B-factor (temperature factor) refinement using the X-PLOR program (*100*, *101*). Diffraction data used in these refinement cycles were gradually increased from 3.0 to 2.5 Å resolution ($F > 2\sigma_F$) in two steps, resulting in a crystallographic R-factor of 0.375. The simulated annealing slow-cool refinement protocol was run from T = 3000 K to T = 277 K in 25 K steps (time step = 0.5 fs, tolerance = 0.2 Å). This refinement was followed by 40 cycles of Powell minimization, 20 cycles of overall B-factor, and 25 cycles of restrained individual B-factor refinement, resulting in an R-factor, of 0.027 for 20−2.5 Å resolution. Difference Fourier maps were calculated at this stage using TOM-FRODO (*101*) and XtalView (*102*); the maps indicated electron density, presumably that of balanol, within the active site of cAPK. A simulated annealed omit map was computed

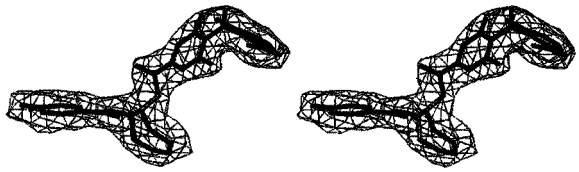

FIGURE 2: Stereoview of balanol electron density. The $F_o - F_c$ map was computed by omitting balanol in structure factor calculations ($R = 0.26$) and is contoured at 6σ (100−102). The mean *B*-factor for balanol's non-hydrogen atoms is 29 Å^2.

by excluding residues within 4.0 Å of the balanol density, and all omitted atoms were fit into the electron density map. Further least-squares refinement was continued with the inclusion of balanol using the conjugate-direction algorithm of the TNT program (*103*). This model was refined to an *R*-factor of 0.20 for data between 20 and 2.5 Å resolution with $F > 1\sigma_F$. The relative orientations of balanol's C and D rings (Figure 1) were ambiguous due to smeared electron density and the absence of the ring D carboxyl group. This ambiguity persisted throughout the X-PLOR and TNT refinements when $2F_o - F_c$ and $F_o - F_c$ electron density difference maps were constructed omitting balanol (*100*, *102*, *103*). A new data set to 2.1 Å resolution was then collected, and the refined model—without balanol—was further refined against this new data with $F > 1\sigma_F$. A difference Fourier map at this stage showed unambiguous electron density for all balanol components (Figure 2). The oxygens of 305 water molecules were assigned to peaks greater than $3\sigma_F$ in the difference Fourier maps, and they formed hydrogen bonds with other polar atoms between 2.3 and 3.5 Å. A final *R* value of 0.202 resulted for the working data set between 20 and 2.1 Å resolution with an R_{free} (*104*) of 0.34 (5% of original data randomly omitted). The computed *R*-factor using all data ($F > 1\sigma_F$) was 21.0%. Residues 1−11 were not observed in the electron density maps and are presumed disordered. The structure's stereochemical parameters were checked with PROCHECK (*105*, *106*). Nonglycine residues are not in disallowed regions of a Ramachandran plot, while 73.8% of nonglycine residues are within the most favored region (*105*−*107*).

RESULTS AND DISCUSSION

Overall Structure. To understand the structural implications of balanol inhibition relative to available biochemical data, balanol was cocrystallized—as opposed to soaked into existing crystals—with the C subunit of cAPK in the absence of metal ions, substrates, and any other inhibitors. The 2.1 Å resolution structure was refined to a crystallographic *R*-factor of 20.2% (Table 1). The rC−balanol crystal structure, depicted in Figure 3, shows similarities to other crystal structures of cAPK complexes. Residues in the large lobe of this structure were superimposed on those of other cAPK complex structures, and the conformational positions of the small lobe relative to the large lobe were compared. These superimpositions indicate that this rC−balanol complex, like that of the rC−adenosine (rC−Ade) complex (*48*), adopts an intermediate conformation between a closed one as reported for the rC−Mn_2ATP−PKI (5−24) complex (*41*) and an open one as reported for the mammalian C (mC) subunit−PKI (5−24) complex (*43*).

More specifically, the radii of gyration in the open (Brookhaven PDB entry 1cmk), intermediate (this structure), and closed (Brookhaven PDB entry 1atp) conformations are, respectively, 21.0, 20.5, and 20.0 Å with respective interlobal distances (as measured between the Nϵ2 atom of His87 and the Oϵ1 atom of Thr197) of 7.1, 4.4, and 2.7 Å. These measurements correlate with the calculated volumes (*41*) of their wedge-shaped active-site clefts (defined as the region bounded by the linker segment, the two lobes and the interpolated surfaces formed at the protein's outer van der Waals limit) observed for the open, intermediate, and closed conformers: 6700, 4800, and 4300 Å^3, respectively. The small lobe in this structure's intermediate conformation is rotated 6° about the linker region relative to the small lobe in the closed conformation (*110*). Least-squares superimposition of large lobe α-carbon atoms in any pair of structures (*110*) representing open, closed, or intermediate conformational states yields an rms deviation of ≤0.5 Å, implying a conserved rigidity in the carboxy-terminal domains of cAPK. The conserved glycine-rich loop and the nonconserevd carboxy-terminal tail (residues 307−350) are ordered with average temperature factors of 34 and 37 Å^2, respectively, for backbone atoms.

Table 1: Data Collection and Structure Determination Statistics

reflections ($F > 1\sigma_F$)	20 045
structure components	3146 total non-hydrogen atoms
enzyme atoms	2801 (residues 12−350)
balanol atoms	40
water oxygen atoms	305
resolution range (Å)	20.0−2.1
R-factor ($\Sigma\|F_o - F_c\|/\Sigma F_o$)	0.202
geometrical parameters (rms deviations)	
general planes (Å)	0.01
trigonal, planes (Å)	0.02
bond lengths (Å)	0.02
bond angles (deg)	2.1

Balanol, as highlighted by an electron density map (Figure 2), fits between the large and small lobes of cAPK, extending from the inner edge to the outer mouth of the active-site cleft (Figure 3). The glycine-rich loop and small lobe provide for tight, induced-fit binding, and the bound balanol extends 17.2 Å from ring A's hydroxyl oxygen atom to the most distant carboxyl oxygen atom of ring D. The four rings of balanol complement the binding subsites of Mg_2ATP with ring A filling the hydrophobic adenine subsite and ring B occupying the ribose subsite (Figure 4). The planar C and D rings, oriented toward cAPK's small lobe, extend the entire length of the glycine-rich loop and mimic metal−phosphate binding (Figure 4). The plane representing the slightly puckered azepane ring of balanol is approximately perpendicular to ring A as is observed in the free balanol structure determined through proton NMR experiments (*81*), and the plane of ring C is nearly orthogonal to that of ring D. The distortions of bound balanol indicate a potential flexibility enabling the inhibitor to adapt to a variety of protein microenvironments. This is expected of an induced-fit ligand that exhibits inhibitory effects against a wide range of kinases.

As a consequence of oxygen-rich ring substituents and of its potentially numerous conformations in the bound state, balanol can surround itself with intermolecular hydrogen bonds for conformational stability and induced-fit binding to a wide variety of protein kinases. In fact, all of balanol's

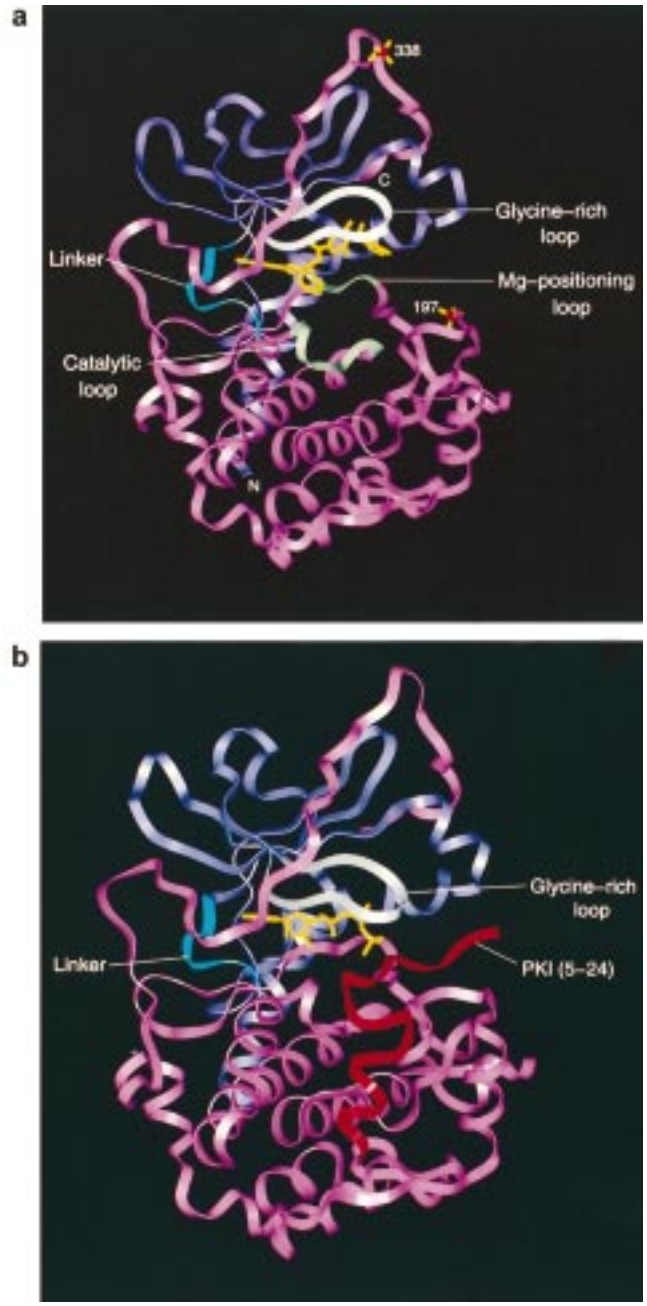

FIGURE 3: Overall structures of the C subunit of cAPK with bound ligands. (a) Depiction of the rC−balanol model. The bi-lobal enzyme is comprised of a small amino-terminal domain (residues 40−120; violet) consisting of a twisted antiparallel five-stranded beta sheet and a larger α-helical domain (residues 128−300; fuschia) interconnected by a short linker segment (residues 121−127; blue). The catalytic and Mg-positioning loops of the large lobe are highlighted in olive. Consistent with kinetic data, balanol (yellow) competes with ATP and fully occupies the active-site cleft between the two lobes of the conserved catalytic core, thus making numerous contacts with the conserved glycine-rich loop (gray) residues of the small lobe. Two phosphate groups are shown: one at Thr197 in the large lobe and one at Ser338. The Ser10 phosphate and amino-terminal residues 1−11 were not observed in the crystal structure. (b) Depiction of the rC−ATP-PKI (5−24) model (*41*). ATP (yellow) is bound in the active site of the C subunit of cAPK (residues 15−350 are represented), making hydrogen bonds to linker segment (blue) and glycine-rich loop (gray) atoms. PKI (residues 5−24), shown in red, binds along the face of the large lobe and extends to the active-site cleft. This figure was produced with Insight II (*108*).

polar atoms are positioned within hydrogen-bonding distance from either enzyme or solvent atoms. Figure 5 summarizes the intermolecular hydrogen-bond network in the rC−balanol complex, including six interacting water molecules. These six water molecules (352−357) are sandwiched within the active-site cleft along one side of balanol.

Balanol Binding. Balanol binds three distinct active-site regions: the adenine subsite, the ribose subsite and the triphosphate subsite. The adenine subsite contains hydrophobic elements, can sterically accommodate one or two cyclic rings, and has the potential to donate and accept electrons in forming hydrogen bonds with bound planar moieties. As indicated by available crystal structures of kinase−ATP mimetic complexes, a planar moiety occupies the adenine subsite. In this reported structure, the cAPK residues whose atoms participate in hydrogen bonds to balanol are the same as those that interact with ATP in the structure of the ternary complex consisting of rC, PKI (5−24), and Mn_2ATP [rC−ATP−PKI (5−24)] (*41*). Specifically, the carbonyl oxygen atom of Glu121 and the backbone nitrogen atom of Val123 form hydrogen bonds in both the rC−balanol and the rC−ATP complexes (Figure 4, Figure 5). In the rC−balanol complex, the single hydroxyl group of balanol's ring A donates and accepts electrons to form hydrogen bonds with these two linker segment atoms; in the rC−ATP−PKI (5−24) complex, the purine ring N1 atom donates electrons to the Val123 amide hydrogen atom while the purine ring N6 atom accepts electrons from the Glu121 backbone carbonyl oxygen atom (Figure 4). ATP mimetics target these backbone atoms in the linker segment and can be anchored within the hydrophobic adenine-binding pocket as a consequence of their planar moieties making favorable nonpolar contacts.

The C subunit's ribose subsite in the rC−balanol complex is occupied by the azepane ring (ring B). Unlike the exocyclic-hydroxyl-containing ribose of ATP, balanol's azepane ring contains only one polar (charged) atom. The azepane ring's N1 atom hydrogen bonds with the backbone carbonyl oxygen atom of the catalytic loop residue Glu170 (Figures 4 and 5). Azepane atoms are involved in favorable nonpolar interactions with Gly50, Glu127, and Glu170 (Table 2). The O1′ and N1′ atoms in the amide linkage between rings A and B hydrogen bond with the side-chain oxygen atom of Thr183 and the oxygen atom of water 352 (Figure 4, Figure 5). The side-chain oxygen atom of Thr183 interacts with the purine N9 atom in the rC−ATP−PKI (5−24) complex. The nonconserved cAPK residues that interact with ring A, ring B, and the amide group interconnecting these rings are Leu49, Ala70, Glu121, Tyr122, Val123, Leu173, Thr183, and Phe327 (Figures 4 and 5, Table 2).

All residues of the glycine-rich loop make nonpolar contact with balanol, and nearly all of these residues possess atoms that hydrogen bond to balanol as well. The majority of these polar and nonpolar interactions involve balanol's benzophenone moiety. These interacting residues comprise the phosphate-binding subsite in the rC−ATP−PKI (5−24) complex. The average temperature factors for backbone atoms of glycine-rich loop residues in this structure approximate those observed in structures of cAPK complexes involving ATP or a nonhydrolyzable ATP analogue. These temperature factors decrease as the number of contacts with an active-site occupant increases. Balanol's ring C and ring D atoms

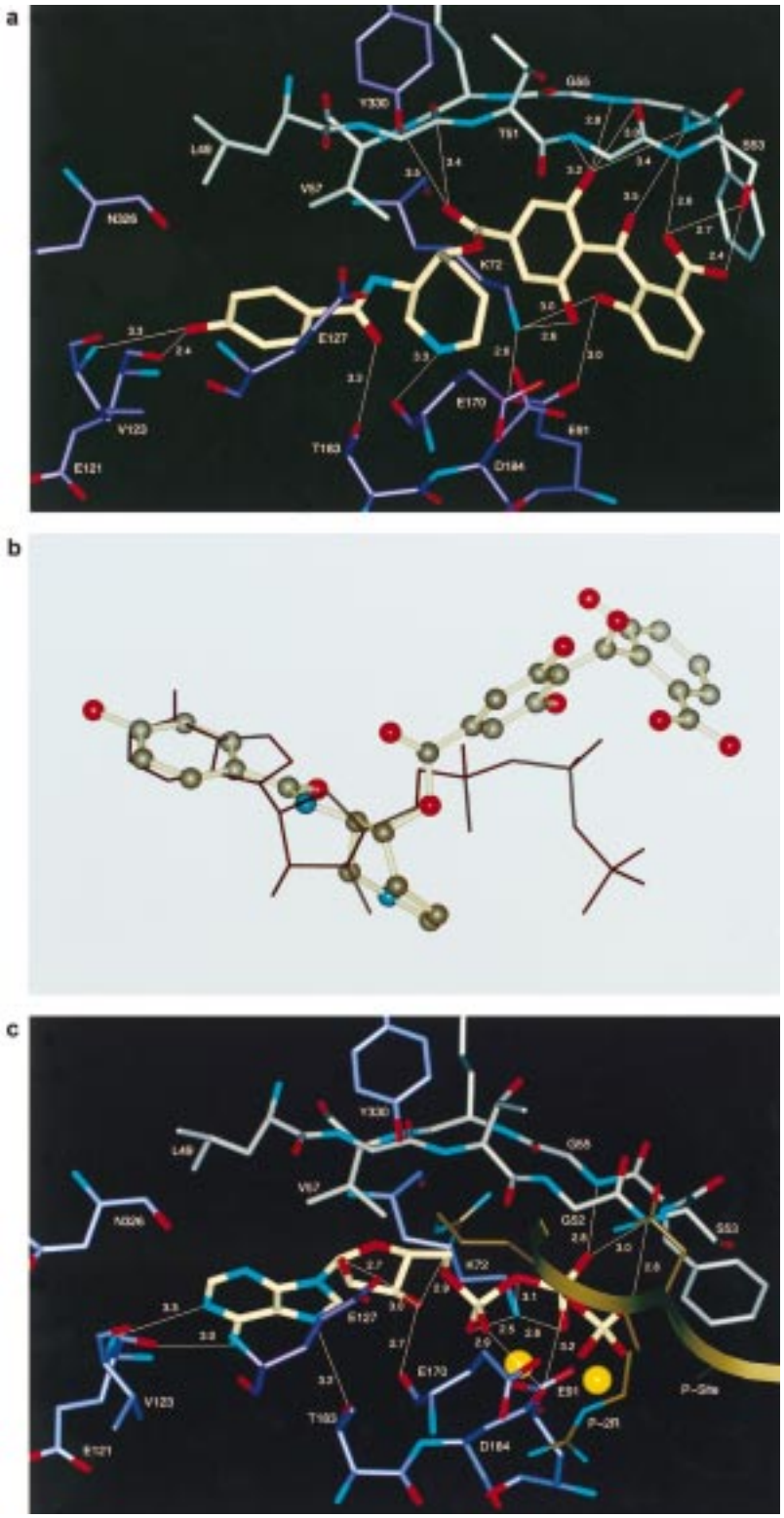

FIGURE 4: Comparison of active site regions. (a) Balanol in the active site as determined in this crystal structure. Carbon atoms of glycine-rich loop residues are light gray with red oxygen atoms and blue nitrogen atoms. Balanol (yellow) extends through the active site with C subunit residues (other than glcine-rich loop ones) depicted with violet. Hydrogen bonds are represented by solidwhite lines between oxygen atoms or between an oxygen and a nitrogen atom with distances noted (*108*). Single letter amino acid codes are used. (b) Superimposition of balanol and ATP as bound conformers. ATP is depicted as a black stick. Balanol is shown as a ball-and-stick model with carbon (gray), oxygen (red) and nitrogen (blue) atoms. This rC−balanol and the rC−ATP-PKI (5−24) crystal structure were superimposed at large lobe residues to determine the relative positions of the bound ligands (*108*). (c) ATP in the active site as determined previously (*41*). Atom coloring and distance markings are the same as those depicted in Figure 4a. Two manganese ions are shown (bright yellow), and four PKI residues (18−21) are shown with a ribbon representing the backbone atoms (brown). For clarity, interactions with the metal ions, though present, are not depicted. Single letter amino acid codes are used. In PKI, the P-site refers to the alanine (residue 21) that replaces the phosphorylatable residue normally found in homologous substrate peptides.

FIGURE 5: Summary of balanol's hydrogen bonds. This ball-and-stick model of balanol and six water molecules (yellow) are spatially illustrated as observed in the crystal structure. One of balanol's 10 oxygen atoms (red), a carboxylate oxygen atom, is shown with a negative charge, while one of balanol's two nitrogen atoms (blue) is shown with a positive charge as expected at neutral pH. Hydrogen bonds were assigned on the basis of measured distances, measured angles and compatibility with other hydrogen bonds (*108*). Hydrogen bonds with water molecules are indicated by black solid lines; all other hydrogen bonds are depicted with black dashed lines.

Table 2: Hydrogen Bonds and van der Waals Interactions Involving Balanol Atoms.

balanol (residue 351) ring name/segment[a]	rC residues or water molecules[b]		total no. of interactions
	H bonds	VDW interactions	
A	V123, E121 (2)	L49, A70, E121, Y122, V123, T183, F327, HOH352 (20)	22
B	E170 (1)	G50, E127, E170, HOH354-356 (10)	11
C	G52, F54, G55, K72, D184 (7)	T51, G52, S53, F54, G55, R56, K72, D184 (32)	39
D	S53, K72, E91, HOH357 (6)	G52, S53, F54, K72, L74, Q84, E91, G186, F187, HOH357 (29)	35
linkers	F54, V57, T183, HOH352, HOH356 (5)	G50, T51, F54, G55, V57, L74, T183, HOH355 (23)	28
totals	21	114	135

[a] Linkers refer to connecting groups of atoms between cyclic rings: the amide between rings A and B, the ester between rings B and C, and the ketone between rings C and D. [b] Hydrogen bonds (≤3.5 Å) and van der Waals interactions (≤4.0 Å) are abbreviated as H bonds and VDW, respectively. Amino acid residues are denoted by one-letter codes and residue numbers. Water molecules are denoted as HOH followed by a specifying number. Integers within parentheses indicate the number of specific interactions. Highly conserved residues are G50, G52, G55, V57, K72, E91, E170, D184, and G186; less-conserved residues are T51, S53, F54, R56, and F187.

interact with highly conserved cAPK residues Gly52, Phe54, Gly55, Lys72, Glu91, Asp184, Gly186, and Phe187 as well as nonconserved residues Leu74 and Gln84 (Table 2). Each of the conserved residues, except Glu91, directly interacts with ATP in the rC−ATP−PKI (5−24) complex, whereas the nonconserved residues do not.

The six ordered water molecules, considered an integral part of bound balanol, are connected via hydrogen bonds (Figure 5). Conserved water molecule 353 (*49*, *111*) forms hydrogen bonds with Leu49, Tyr330, and water 352. Balanol also makes water-mediated contacts with cAPK residues: balanol's N1′ atom interacts with the hydroxyl group of Tyr330 via two bridging water molecules, and water molecules 356 and 357 form hydrogen bonds with balanol oxygen atoms of the ester linkage and ring D carbonyl, respectively (Figure 5). Tight and specific binding of balanol, however, cannot be explained by favorable hydrogen-bond interactions (*96*). The predominant nonpolar interactions between balanol and its complementary bound-state environment (Table 2) contribute most to the potency of balanol against protein kinases (*95*, *96*). The benzophenone rings of balanol are positioned adjacent to the glycine-rich loop and distant from the catalytic loop, so the majority of favorable polar and nonpolar interactions occur with small lobe residues.

Protein−Ligand Interactions. In addition to specific hydrogen bonds, hydrophobic effects, and van der Waals interactions, the affinity of proteins for ligands depends on shape complementarity and ionic interactions. In this rC−balanol structure, ionic interactions are negligible. Shape complementarity includes steric factors and, in this report's complex, occurs as a consequence of a flexible ligand, a pivotable linker segment, and a glycine-rich loop capable of extensive ligand complementarity. In addition to currently available crystal structures, this crystal structure helps explain observed potent inhibition of cAPK by depicting the numerous key intermolecular interactions underlying balanol's potency and specificity. This structure of an rC−ATP mimetic complex, in the absence of a substrate peptide and other inhibitors, permits evaluation of the conformational changes occurring in the enzyme solely due to protein−inhibitor interactions.

We expect the polar and nonpolar environments presented by active-site regions of the protein kinases potently inhibited

by balanol (*95*) to be topologically similar with some noteworthy positional exceptions. This concept becomes more obvious when one focuses on specific side chains and their conformational states. Specifically, the flexible and complementary side chains of Ser53 and Phe54 adopt significantly different positions in this structure relative to those observed in the structurally intermediate rC−Ade conformer (*48*), the closed rC−ATP−PKI (5−24) structure (*41*) and the mC−staurosporine−PKI (5−24) complex (*49*). The rearrangement of the Phe54 and Ser53 side chains in the rC−balanol complex appears to sterically accommodate balanol's ring D and enable favorable polar and nonpolar contacts. Stacking of Phe54's side-chain ring onto balanol's ring D may appear to be an important factor underlying balanol's inhibition specificity; however, the measured affinity for balanol of a cAPK mutant in which Phe54 was replaced with glycine is unchanged compared to wild-type rC, as discussed in an accompanying report (*95*). In this structure, the side chain of Phe54 (mean *B*-factor of 47 Å^2) makes nonpolar contacts with the well-ordered B-helix residue Val79 (mean *B*-factor of 15 Å^2) and the C-helix residue Gln84 (mean *B*-factor of 47 Å^2). These latter two residues appear to stabilize Phe54 and, therefore, Phe54's interaction with balanol ring D.

Like Phe54's side chain, Ser53's side chain in this structure is tucked in to the active site beneath glycine-rich loop backbone atoms as opposed to a more extended and exposed position observed in both the rC−Ade and rC−ATP−PKI (5−24) structures. Ser53's backbone amide hydrogen bonds to balanol, and Ser53's side-chain oxygen atom makes two hydrogen bonds with balanol (Figures 4 and 5). In the cAPK−staurosporine complex (*49*), the side chain of Phe54 is folded even further under the glycine-rich loop compared to its position in this rC−balanol structure. While the side chains of Phe54 and Ser53 may not be critically responsible for the observed high affinity of protein kinases for balanol, the interactions of these side chains with bound ligands do rigidify glycine-rich loop residues in all cAPK-ligand crystal structures.

The eight hydrogen bonds made with balanol by glycine-rich loop backbone oxygen and amide hydrogen atoms appear to be more important for binding (Figures 4 and 5). An additional three hydrogen bonds are made indirectly by these backbone atoms through conserved bridging water molecules. Besides Ser53, only four cAPK residues have side chains that form hydrogen bonds with balanol: side chain atoms of Lys72, Glu91, Thr183, and Asp184 make six hydrogen bonds with balanol. Of these four residues, all but Thr183 are highly conserved. In other words, balanol exhibits particular complementarity to the active site of cAPK at the level of conserved residues. Still, polar interactions have not been determined to account solely for balanol's specificity and high affinity toward protein kinases (*96*).

As noted previously, the structure of this rC−inhibitor complex in the absence of a substrate peptide or other inhibitors thus permits evaluation of enzyme conformational changes stemming only from protein−inhibitor interactions. In cAPK complexes involving the H series of protein kinase inhibitors, the isoquinolinesulfonyl nitrogen atoms form hydrogen bonds to the backbone amide of Val123 but not to Glu121 (*45*). The numerous interactions between these H-series inhibitors and the C subunit are mostly nonpolar, and the intermolecular contacts between H-series inhibitors and Phe327 of cAPK's carboxy-terminal tail is considered important for selectivity (*45*). The natural product staurosporine potently inhibits cAPK and other protein kinases (*112*−*114*). Staurosporine consists primarily of fused aromatic rings that avoid steric clashes with the side chains of protein kinase residues. The amide-containing lactam and carbonyl groups of staurosporine can donate and accept electrons in forming hydrogen bonds with linker segment atoms. Like balanol, staurosporine utilizes extensive nonpolar interactions to achieve potent, induced-fit inhibition (*49*).

In contrast, olomoucine is a cyclin-dependent kinase 2 (cdk2) inhibitor comprised of substituents that would sterically interfere with similar binding by cAPK; olomoucine is not observed to inhibit cAPK (*115*, *116*). Crystal structures of the fibroblast growth factor (FGF) receptor tyrosine kinase domain in complex with oxindole inhibitors also show adenine-binding-pocket interactions (*72*). The FGF−oxindole inhibitor structures, however, indicate that these inhibitors contain substituents that protrude from the side of the active-site cleft (*72*) instead of extensively complementing the cleft's glycine-rich loop as in this cAPK−balanol structure. The bound conformations of the oxindole inhibitors would be unfavorable were they to form a complex with cAPK, since, again, inhibitor substituents would sterically clash with the side chains of cAPK active-site residues.

CONCLUDING REMARKS

The adenine-binding pocket makes several contacts that confer stability to the inhibitor-bound complex. In fact, all protein kinase crystal structures solved to date as complexes with ATP mimetics identify interactions between the ligand and the adenine subsite. Balanol's ring A and ring A's hydroxyl substituent occupy this subsite. However, more than occupation of this hydrophobic pocket is required for the inhibition specificity and potency observed against diverse protein kinases (*95*). Within the subset of kinase crystal structures involving potent inhibitors, polar and nonpolar interactions involve binding regions distinct from the adenine subsite (Table 2). Two other binding regions, the ribose subsite and the triphosphate subsite, have been described. In this rC−balanol structure, the ribose subsite of cAPK envelopes balanol's azepane ring and the amide linkage to balanol's ring A. Within the triphosphate subsite of cAPK, the majority of both the polar and nonpolar protein−ligand interactions occur; balanol's ester linkage and benzophenone moiety occupy this subsite.

These three binding regions can also be classified according to their functions of identification, accommodation, and inhibition. In the apoenzyme, cAPK is expected to adopt an open conformation, thereby enabling the adenine-binding pocket to identify potential ligands. The adenine subsite can serve as an anchor point to orient the ligand for binding within the remaining two binding regions; ligand interactions with cAPK's linker segment predominate within the adenine subsite. This hypothesized initial recognition event could trigger cAPK's transformation from an open conformation to the intermediate or closed conformations observed in crystal structures of complexes involving bound active-site ligands. This proposed mechanism is consistent with chemical footprinting studies involving the free catalytic subunit

and a complex of the catalytic subunit with Mg_2ATP: binding of Mg_2ATP is sufficient to induce a closed conformation for the catalytic subunit (*117*).

The ribose subsite must next accommodate the ribose-like moiety linking the adenine-like portion of a potential ligand to the ligand's phosphate-like groups. Polar and nonpolar interactions within the ribose-binding subsite occur with both large and small lobe cAPK residues, thus further sequestering the ligand within the active site and promoting active-site closure. With nearly half of balanol's atoms being dragged into, accommodated, and oriented within the active site of cAPK, the remaining half of balanol's atoms are primed for high-affinity binding at the triphosphate subsite. The triphosphate subsite spans nearly the full length of the antiparallel strands that comprise the glycine-rich loop. Two-thirds of balanol's polar and nonpolar interactions occur with residues of the triphosphate subsite. Although a very similar pattern is observed with Mn_2ATP binding, three important differences are depicted in Figure 4.

The volume of cAPK's active site correlates with its interlobal distance as discussed previously. Differences between the rC−balanol and rC−ATP−PKI (5−24) active-site regions are readily apparent (Figure 4), especially when one focuses on distances between the glycine-rich loop residues (above) and both catalytic and Mg positioning loops (below). Mg_2ATP orients the glycine-rich loop of cAPK's small lobe toward the large lobe's catalytic loop where residues that participate in phosphoryl transfer are situated. In contrast, balanol orients the glycine-rich loop away from the large lobe, thereby further opening the active-site cleft. In this position, residues of the catalytic loop are much more solvent accessible. The second important structural difference between the rC−balanol and rC−ATP−PKI (5−24) structural complexes is that balanol binding results in a compression of the small lobe, as evidenced by the 2.7 Å distance between Lys72 and Glu91. This distance is less than that observed in any other cAPK catalytic subunit structure. Another important structural difference between the rC−balanol and rC−ATP−PKI (5−24) structural complexes is the conformation of the glycine-rich loop. In the rC−ATP−PKI (5−24) structure, the glycine-rich loop appears stretched out and extended. In the rC−balanol structure, the glycine-rich loop adopts a more puckered conformation; Ser53 and Phe54 side chains tuck partially under the glycine-rich loop to interact with balanol. These two side chains in the rC−ATP−PKI (5−24) structure, however, stretch out and interact with PKI residues. An additional important difference between the rC−ATP−PKI (5−24) and rC−balanol structures relates to the number of ligands present. In addition to ATP, two metal ions and four PKI residues make numerous polar and nonpolar contacts with cAPK residues in the rC−ATP−PKI (5−24) complex. These additional ligands also interact with ATP, the primary active-site occupant. Not only does balanol mimic ATP binding but it also replaces three other active-site ligands, each possessing a unique affinity for cAPK. The presence of these additional ligands and their respective affinities may or may not add in a mathematically associative manner. This contributes to the biochemical difficulties of dissecting the active site of cAPK catalytic events down to their most fundamental components. Nonetheless, specific contributions to the energetic determinants of balanol binding can be rigorously analyzed with some assumptions, and such an analysis is the focus of an accompanying paper (*96*). In closing, comprehensive analyses of balanol derivatives that differ markedly in their affinities and specificities for PKC isoforms and cAPK further suggest that cAPK is generally more sensitive to alterations within the ribose subsite, whereas PKC isoforms tend to be more sensitive to derivatizations to the benzophenone moiety occupying the triphosphate subsite. These empirical observations and our reported structure thus provide a basis for probing the underlying specific molecular interactions between balanol and members of the cAPK, PKC, and PKG family of protein kinases.

ACKNOWLEDGMENT

We specifically thank S. Cox, P. H. Hünenberger, E. Radzio-Andzelm, D. B. Huang, S. Dempsey, Madhusudan, R. Aimes, and S. Garrod for assistance and helpful discussions. We thank V. Ashford, C. Nielsen, D. Sullivan, and N. Nguyen for support at the multiwire-area detector facility of the NIH National Research Resource at UCSD. Raja Elhayek assisted with growing crystals, and computing time was utilized for X-PLOR and TNT refinements at the San Diego Supercomputer Center. We are also grateful to the experts at Award Photo Imaging, San Diego, CA, for their tireless photographic service in support of our color illustration efforts.

REFERENCES

1. Hanks, S. K., Quinn, A. M., and Hunter, T. (1988) *Science 241*, 42.
2. Hunter, T. (1991) *Methods Enzymol. 200*, 3.
3. Hanks, S. K., and Quinn, A. M. (1991) *Methods Enzymol. 200*, 38.
4. Lindberg, R. A., Quinn, A. M., and Hunter, T. (1992) *Trends Biochem. Sci. 17*, 114.
5. Taylor, S. S., Knighton, D. R., Zheng, J., Sowadski, J. M., Gibbs, C. S., and Zoller, M. J. (1993) *Trends Biochem. Sci. 18*, 84.
6. Hanks, S. K., and Hunter, T. (1995) *FASEB J. 9*, 576.
7. Krebs, E. G., Graves, D. J., and Fischer, E. H. (1959) *J. Biol. Chem. 234*, 2867.
8. Castagna, M., Takai, Y., Kaibuchi, K., Sano, K., Kikkawa, U., and Nishizuka, Y. (1982) *J. Biol. Chem. 257*, 7847.
9. Nishizuka, Y. (1984) *Nature 308*, 693.
10. Nishizuka, Y. (1988). *Nature 334*, 661.
11. Farago, A., and Nishizuka, Y. (1990) *FEBS Lett. 268*, 350.
12. Jakobovits, A., Rosenthal, A., and Capon, D. J. (1990) *EMBO J. 9*, 1165.
13. Nigg, E. A. (1990) *Adv. Cancer Res. 55*, 271.
14. Meinkoth, J. L., Ji, Y., Taylor, S. S., and Feramisco, J. R. (1990) *Proc. Natl Acad. Sci. U.S.A. 87*, 9595.
15. Zetterqvist, Ö. Z., Ragnarsson, U., and Engström, L. (1990) in *Peptides and Protein Phosphorylation* (Kemp, B. E., Ed.) pp 171−187, CRC Press, Inc., Boca Raton, FL.
16. Wu, J., Dent, P., Jelinek, T., Wolfman, A., Weber, M. J., and Sturgill, T. W. (1993) *Science 262*, 1065.
17. Cook, S. J., and McCormick, F. (1993) *Science 262*, 1069.
18. Newton, A. C. (1993) *Annu. Rev. Biophys. Biomol. Struct. 22*, 1.
19. Pepinsky, R. B., and Sinclair, L. K. (1986) *Nature 321*, 81.
20. Touqui, L., Rothhut, B., Shaw, A. M., Fradin, A., Vargaftig, B. B., and Russo-Marie, F. (1986) *Nature 321*, 177.
21. Tritton, T. R., and Hickman, J. A. (1990) *Cancer Cells 2*, 95.
22. Bradshaw, D., Hill, C. H., Nixon, J. S., and Wilkinson, S. E. (1993) *Agents Actions 38*, 135.
23. Lee, J. C., Laydon, J. T., McDonnell, P. C., Gallagher, T. F., Kumar, S., Green, D., McNulty, D., Blumenthal, M. J., Heys, J. R., and Landvatter, S. W. (1994) *Nature 372*, 739.

24. Ishii, H., Jirousek, M. R., Koya, D., Takagi, C., Xia, P., Clermont, A., Bursell, S. E., Kern, T. S., Ballas, L. M., Heath, W. F., Stramm, L. E., Feener, E. P., and King, G. L. (1996) *Science 272*, 728.
25. Mildvan, A. S., Kaiser, E. T., Rosevear, P. R., and Bramson, H. N. (1984) *Fed. Proc. 43*, 2634.
26. Bramson, H. N., Kaiser, E. T., and Mildvan, A. S. (1984) *CRC Crit. Rev. Biochem. 15*, 93.
27. Beebe, S., Corbin, J. D. (1986) in *The Enzymes: Control by Phosphorylation, Part A (Vol. XVII)* (Krebs, E. G., and Boyer, P. D., Eds.) pp 43−111, Academic Press, New York.
28. Taylor, S. S., Bubis, J., Toner-Webb, J., Saraswat, L. D., First, E. A., Buechler, J. A., Knighton, D. R., and Sowadski, J. (1988) *FASEB J. 2*, 2677.
29. Taylor, S. S., Buechler, J. A., and Yonemoto, W. (1990) *Annu. Rev. Biochem. 59*, 971.
30. Taylor, S. S., Buechler, J. A., and Knighton, D. R. (1990) in *Peptides and Protein Phosphorylation* (Kemp, B. E., Ed.) pp 1−42, CRC Press, Boca Raton, FL.
31. Taylor, S. S., Knighton, D. R., Zheng, J., Ten Eyck, L. F., and Sowadski, J. M. (1992) *Annu. Rev. Cell Biol. 8*, 429.
32. Kemp, B. E., Graves, D. J., Benjamini, E., and Krebs, E. G. (1977) *J. Biol. Chem. 252*, 4888.
33. Herberg, F. W., Bell, S. M., and Taylor, S. S. (1993) *Protein Eng. 6*, 771.
34. Cheng, H.-C., Van Patten, S. M., Smith, A. J., and Walsh, D. A. (1985) *Biochem. J. 231*, 655.
35. Walsh, D. A., Angelos, K. L., van Patten, S. M., Glass, D. B., and Garetto, L. P. (1990) in *Peptides and Protein Phosphorylation* (Kemp, B. E., Ed.) pp 43−84, CRC Press, Inc., Boca Raton, FL.
36. Knighton, D. R., Zheng, J. H., Ten Eyck, L. F., Ashford, V. A., Xuong, N.-H., Taylor, S. S., and Sowadski, J. M. (1991) *Science 253*, 407.
37. Knighton, D. R., Zheng, J. H., Ten Eyck, L. F., Xuong, N.-H., Taylor, S. S., and Sowadski, J. M. (1991) *Science 253*, 414.
38. Bossemeyer, D., Engh, R. A., Kinzel, V., Ponstingl, H., and Huber, R. (1993) *EMBO J. 12*, 849.
39. Karlsson, R., Zheng, J., Xuong, N.-H., Taylor, S. S., and Sowadski, J. M. (1993) *Acta Crystallogr., Sect. D 49*, 381.
40. Knighton, D. R., Bell, S. M., Zheng, J., Ten Eyck, L. F., Xuong, N.-H., Taylor, S. S., and Sowadski, J. M. (1993) *Acta Crystallogr., Sect. D 49*, 357.
41. Zheng, J., Trafny, E. A., Knighton, D. R., Xuong, N.-H., Taylor, S. S., Ten Eyck, L. F., and Sowadski, J. M. (1993) *Acta Crystallogr., Sect. D 49*, 362.
42. Zheng, J., Knighton, D. R., Ten Eyck, L. F., Karlsson, R., Xuong, N.-H., Taylor, S. S., and Sowadski, J. M. (1993) *Biochemistry 32*, 2154.
43. Zheng, J., Knighton, D. R., Xuong, N.-H., Taylor, S. S., Sowadski, J. M., and Ten Eyck, L. F. (1993) *Protein Sci. 2*, 1559.
44. Madhusudan, Trafny, E. A., Xuong, N.-H. Adams, J. A., Ten Eyck, L. F., Taylor, S. S., and Sowadski, J. M. (1994) *Protein Sci. 3*, 176.
45. Engh, R. A., Girod, A., Kinzel, V., Huber, R., and Bossemeyer, D. (1996) *J. Biol. Chem. 271*, 26157.
46. Sowadski, J. M., Ellis, C. A., and Madhusudan (1996) *J. Bioeng Biomed. 28*, 7.
47. Narayana, N., Cox, S., Shaltiel, S., Taylor, S. S., and Xuong, N.-H. (1997) *Biochemistry 36*, 4438.
48. Narayana, N., Cox, S., Xuong, N.-H., Ten Eyck, L. F., and Taylor, S. S. (1997) *Structure 5*, 921.
49. Prade, L., Engh, R. A., Girod, A., Kinzel, V., Huber, R., and Bossemeyer, D. (1997) *Structure 5*, 1627.
50. Toledo, L. M., and Lydon, N. B. (1997) *Structure 5*, 1551.
51. Knighton, D. R., Pearson, R. B., Sowadski, J. M., Means, A. R., Ten Eyck, L. F., Taylor, S. S., and Kemp, B. E. (1992) *Science 258*, 130.
52. De Bondt, H. L., Rosenblatt, J., Jancarik, J., Jones, H. D., Morgan, D. O., and Kim, S.-H. (1993) *Nature 363*, 595.
53. Hu, S. H., Parker, M. W., Lei, J. Y., Wilce, M. C., Benian, G. M., and Kemp, B. E. (1994) *Nature 369*, 581.
54. Hubbard, S. R., Wei, L., Ellis, L., and Hendrickson, W. A. (1994) *Nature 372*, 746.
55. Owen, D. J., Noble, M. E., Garman, E. F., Papageorgiou, A. C., Johnson, L. N. (1995) *Structure 3*, 467.
56. Xu, R. M., Carmel, G., Sweet, R. M., Kuret, J., Cheng, X. (1995) *EMBO J. 14*, 1015.
57. Lee, C.-H., Saksela, K., Mirza, U. A., Chait, B. T., and Kuriyan, J. (1996). *Cell 85*, 931.
58. Longenecker, K. L., Roach, P. J., and Hurley, T. D. (1996) *J. Mol. Biol. 257*, 618.
59. Russo, A. A., Jeffrey, P. D., and Pavletich, N. P. (1996) *Nat. Struct. Biol. 3*, 696.
60. Wilson, K. P., Fitzgibbon, M. J., Caron, P. R., Griffith, J. P., Chen, W., McCaffrey, P. G., Chambers, S. P., and Su, M. S. S. (1996) *J. Biol. Chem. 271*, 27696.
61. Sicheri, F., Moarefi, I., and Kuriyan, J. (1997) *Nature 385*, 602.
62. Xu, W., Harrison, S. C., and Eck, M. J. (1997) *Nature 385*, 595.
63. Canagarajah, B. J., Khokhlatchev, A., Cobb, M. H., and Goldsmith, E. J. (1997) *Cell 90*, 859.
64. Hon, W.-C., McKay, G. A., Thompson, P. R., Sweet, R. M., Yang, D. S., Wright, G. D., and Berghuis, A. M. (1997) *Cell 89*, 887.
65. Wang, Z., Harkins, P. C., Ulevitch, R. J., Han, J., Cobb, M. H., and Goldsmith, E. J. (1997) *Proc. Natl Acad. Sci. U.S.A. 94*, 2327.
66. Schulze-Gahmen, U., Brandsen, J., Jones, H. D., Morgan, D. O., Meijer, L., Vesely, J., and Kim, S.-H. (1995) *Proteins* 22, 378.
67. Russo, A. A., Jeffrey, P. D., Patten, A. K., Massagué, J., and Pavletich, N. P. (1996) *Nature 382*, 325.
68. De Azevedo, W. F., Jr., Mueller-Dieckmann, H. J., Schulze-Gahmen, U., Worland, P. J., Sausville, E., and Kim, S.-H. (1996) *Proc. Natl Acad. Sci. U.S.A. 93*, 2735.
69. Schulze-Gahmen, U., De Bondt, H. L., and Kim, S.-H. (1996) *J. Med. Chem. 39*, 4540.
70. De Azevedo, W. F., Leclerc, S., Meijer, L., Havlicek, L., Strnad, M., and Kim, S.-H. (1997) *Eur. J. Biochem. 243*, 518.
71. Lawrie, A. M., Noble, M. E., Tunnah, P., Brown, N. R., Johnson, L. N., and Endicott, J. A. (1997) *Nat. Struct. Biol. 4*, 796.
72. Mohammadi, M., McMahon, G., Sun, L., Tang, C., Hirth, P., Yeh, B. K., Hubbard, S. R., and Schlessinger, J. (1997) *Science 276*, 955.
73. Singh, J., Dobrusin, E. M., Fry, D. W., Haske, T., Whitty, A., and McNamara, D. J. (1997) *J. Med. Chem. 40*, 1130.
74. Tong, L., Pav, S., White, D. M., Rogers, S., Crane, K. M., Cywin, C. L., Brown, M. L., and Pargellis, C. A. (1997) *Nat. Struct. Biol. 4*, 311.
75. Wilson, K. P., McCaffrey, P. G., Hsiao, K., Pazhanisamy, S., Galullo, V., Bemis, G. W., Fitzgibbon, M. J., Caron, P. R., Murcko, M. A., and Su, M. S. S. (1997) *Chem. Biol. 4*, 423.
76. Blundell, T. L., Sibanda, B. L., Sternberg, M. J. E., and Thornton, J. M. (1987) *Nature 326*, 347.
77. Rutenber, E., Fauman, E. B., Keenan, R. J., Fong, S., Furth, P. S., Ortiz de Montellano, P. R., Meng, E., Kuntz, I. D., DeCamp, D. L., and Salto, R. (1993) *J. Biol. Chem. 268*, 15343.
78. Kuntz, I. D., Meng, E. C., and Schoichet, B. K. (1994) *Acc. Chem. Res. 27*, 117.
79. Colman, P. M. (1994) *Curr. Opin. Struct. Biol. 4*, 868.
80. ChemDraw Plus, Version 3.1 (1993) Cambridge Scientific Computing Inc., Cambridge, MA.
81. Kulanthaivel, P., Hallock, Y. F., Boros, C., Hamilton, S. M., Janzen, W. P., Ballas, L. M., Loomis, C. R., Jiang, J. B., Katz, B., Steiner, J. R., and Clardy, J. (1993) *J. Am. Chem. Soc. 115*, 6452.
82. Kneifel, H., König, W. A., Loeffler, W., and Müller, R. (1977) *Arch. Microbiol. 113*, 121.
83. König, W. A., Sinnwell, V., Witt, S., and Kneiffel, H. (1980) *Chem. Ber. 113*, 2221.
84. Boros, C., Hamilton, S. M., Katz, B., and Kulanthaivel, P. (1994) *J. Antibiot. 47*, 1010.

85. Ohshima, S., Yanagisawa, M., Katoh, A., Fujii, T., Sano, T., Matsukuma, S., Furumai, T., Fujiu, M., Watanabe, K., and Yokose, K. (1994). *J. Antibiot. 47*, 639.
86. Nicolaou, K. C., Bunnage, M. E., and Koide, K. (1994) *J. Am. Chem. Soc. 116*, 8402.
87. Lampe, J. W., Hughes, P. F., Biggers, C. K., Smith, S. H., and Hu, H. (1994) *J. Org. Chem. 59*, 5147.
88. Nicolaou, K. C., Koide, K., and Bunnage, M. E. (1995) *Chem Eur. J. 1*, 454.
89. Adams, C. P., Fairway, S. M., Hardy, C. J., Hibbs, D. E., Hursthouse, M. B., Morley, A. D., Sharp, B. W., Vicker, N., and Warner, I. (1995) *J. Chem. Soc., Perkin Trans. 1*, 2355.
90. Lampe, J. W., Hughes, P. F., Biggers, C. K., Smith, S. H., and Hu, H. (1996) *J. Org. Chem. 61*, 4572.
91. Koide, K., Bunnage, M. E., Gomez Paloma, L., Kanter, J. R., Taylor, S. S., Brunton, L. L., and Nicolaou, K. C. (1995) *Chem. Biol. 2*, 601.
92. Mendoza, J. S., Jagdmann, G. E., Jr., and Gosnell, P. A. (1995) *Bioorg. Med. Chem. Lett. 5*, 2211.
93. Defauw, J. M., Murphy, M. M., Jagdmann, G. E., Jr.; Hu, H., Lampe, J. W., Hollinshead, S. P., Mitchell, T. J., Crane, H. M., Heerding, J. M., Mendoza, J. S., Davis, J. E., Darges, J. W., Hubbard, F. R., and Hall, S. E. (1996) *J. Med. Chem. 39*, 5215.
94. Lai, Y. S., Mendoza, J. S., Jagdmann, G. E., Jr., Menaldino, D. S., Biggers, C. K., Heerding, J. M., Wilson, J. W., Hall, S. E., Jiang, J. B., Janzen, W. P., Ballas, L. M., (1997) *J. Med. Chem. 40*, 226.
95. Setyawan, J., Koide, K., Diller, T. C., Taylor, S. S., Nicolaou, K. C., and Brunton, L. L. (1999) (Submitted for publication).
96. Hünenberger, P. H., Helms, V., Narayana, N., Taylor, S. S., and McCammon, J. (1999) *Biochemistry 38*, 2358−2366.
97. Hamlin, R. (1985) *Methods Enzymol. 114A*, 416.
98. Howard, A. J., Nielsen, C., and Xuong, N.-H. (1985) *Methods Enzymol. 114A*, 452.
99. Brünger, A. T., Kuriyan, J., and Karplus, M. (1987) *Science 235*, 458.
100. Brünger, A. T. (1992) In *X-PLOR Version 3.1: A System for X-ray and NMR*, Yale University Press, New Haven, CT.
101. Cambillau, C., and Horjales, E. (1987) *J. Mol. Graph. 5*, 174.
102. McRee, D. E. (1992) *J. Mol. Graph. 10*, 44.
103. Tronrud, D. E., Ten Eyck, L. F., and Matthews, B. W. (1987) *Acta Crystallogr., Sect. A 43*, 489.
104. Brünger, A. T. (1992) *Nature 355*, 472.
105. Laskowski, R. A., MacArthur, M. W., Moss, D. S., and Thornton, J. M. (1993) *J. Appl. Crystallogr. 26*, 283.
106. Laskowski, R. A., Moss, D. S., and Thornton, J. M. (1993) *J. Mol. Biol. 231*, 1049.
107. Ramachandran, G. N., and Sasisekharan, V. (1968) *Adv. Protein Chem. 23*, 283.
108. Insight II, Version 97.0 (1997), Molecular Modeling System, Molecular Simulations Inc., San Diego, CA.
109. Laskowski, R. A. (1995) *J. Mol. Graph. 13*, 323.
110. Diamond, R. (1992) *Protein Sci. 1*, 1279.
111. Shaltiel, S., Cox, S., and Taylor, S. S. (1998). *Proc. Natl Acad. Sci. U.S.A. 95*, 484.
112. Tamaoki, T., Nomoto, H., Takahashi, I., Kato, Y., Morimoto, M., and Tomita, F. (1986) *Biochem. Biophys. Res. Commun. 135*, 397.
113. Herbert, J. M., Seban, E., and Maffrand, J. P. (1990) *Biochem. Biophys. Res. Commun. 171*, 189.
114. Yanagihara, N., Tachikawa, E., Izumi, F., Yasugawa, S., Yamamoto, H., and Miyamoto, E. (1991) *J. Neurochem. 56*, 294.
115. Vesely, J., Havlicek, L., Strnad, M., Blow, J. J., Donella-Deana, A., Pinna, L., Letham, D. S., Kato, J., Detivaud, L., and Leclerc, S. (1994) *Eur. J. Biochem. 224*, 771.
116. Havlícek, L., Hanus, J., Vesely, J., Leclerc, S., Meijer, L., Shaw, G., and Strnad, M. (1997) *J. Med. Chem. 40*, 408.
117. Cheng, X., Shaltiel, S., and Taylor, S. S. (1998) *Biochemistry 37*, 140005.

BI9820659